Multi-scale 2D Temporal Map Diffusion Models for Natural Language Video Localization

Chongzhi Zhang[1,4], Mingyuan Zhang[1,4], Zhiyang Teng[2,*], Jiayi Li[4], Xizhou Zhu[3], Lewei Lu[3], Ziwei Liu[1,4], Aixin Sun[1,4,✉]
[1]S-Lab, Nanyang Technological University [2]ByteDance [3]SenseTime
[4]School of Computer Science and Engineering, Nanyang Technological University
{chongzhi001, mingyuan001, jli10}@e.ntu.edu.sg, chihyangteng@gmail.com,
{zhuxizhou, luotto}@sensetime.com, {axsun, ziwei.liu}@ntu.edu.sg

Abstract

Natural Language Video Localization (NLVL), grounding phrases from natural language descriptions to corresponding video segments, is a complex yet critical task in video understanding. Despite ongoing advancements, many existing solutions lack the capability to globally capture temporal dynamics of the video data. In this study, we present a novel approach to NLVL that aims to address this issue. Our method involves the direct generation of a global 2D temporal map via a conditional denoising diffusion process, based on the input video and language query. The main challenges are the inherent sparsity and discontinuity of a 2D temporal map in devising the diffusion decoder. To address these challenges, we introduce a multi-scale technique and develop an innovative diffusion decoder. Our approach effectively encapsulates the interaction between the query and video data across various time scales. Experiments on the Charades and DiDeMo datasets underscore the potency of our design.

1. Introduction

Natural Language Video Localization (NLVL) is an essential and significant task in the field of video understanding, boasting a variety of application opportunities. Given an untrimmed video and a query sentence, the NLVL task is to retrieve a temporal moment that semantically corresponds to the query. The top part of Fig. 1 provides an example of the NLVL task, where the NLVL model returns the start and end time stamps of a video moment in response to the query "a person sits in a chair".

Several methods have been proposed to tackle the NLVL task. Regression-based methods [5, 18, 36] directly estimate the temporal timing of target moments by leveraging cross-modal interactions between videos and queries. Span-based methods [9, 13, 38, 39] approach NLVL as a span prediction task, predicting the likelihood of each video segment being the start and end of the target moment. Proposal-based methods [30–32] generate candidate moments, then select

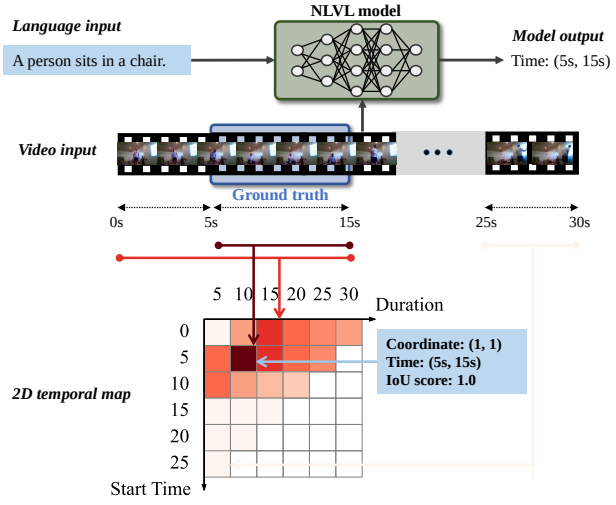

Figure 1. Illustration of the NLVL task (top part) and 2D temporal map (bottom part). Top: The NLVL model processes a language query and an untrimmed video to locate a temporal moment that semantically corresponds to the query. Bottom: The 2D temporal map plots candidate moments at coordinates (i, j), starting at $i\tau$ and lasting for $(j+1)\tau$; here $\tau = 5$s is the time scale. The map is displayed as a heatmap, where the values in cells indicate the predicted matching scores between candidate moments and the target moment. Note that the "ground truth" in the figure is for illustration purpose, and is not available during model inference.

[*]Work done while at S-Lab.
[✉]Corresponding author.

the most relevant proposal for a given query. Among the latter, 2D-Map methods [29, 42] utilize a two-dimensional map to represent temporal relationships among proposals. In a 2D temporal map with τ as the time unit, the coordinates (i, j) indicate a candidate moment starting at $i\tau$ and lasting for $(j+1)\tau$, as shown in the bottom part of Fig. 1. This representation captures all feasible proposals of varying lengths and maintains their adjacent relationships. By including data from neighboring moments, the model is able to gain a comprehensive view of video content, enhancing its understanding and prediction of temporal relationships.

Unlike traditional approaches that treat NLVL as an understanding problem, we frame it as a generative task, using a multi-scale 2D temporal map diffusion model. That is, we adopt a novel perspective on the NLVL task, leveraging the capabilities of diffusion models, a class of generative models renowned for their success in image and text generation. The diffusion model operates on the principle of systematically perturbing data through a forward diffusion process and subsequently recovering the original data via a learned reverse diffusion process. Accordingly, our approach reimagines the NLVL task as the generation of a 2D temporal map, conditioned on both video and language inputs.

Here, the fundamental differences between generative and understanding tasks present unique challenges in designing an effective diffusion decoder. To this end, we have developed a specialized condition-injected decoder, featuring a meticulously crafted architecture that seamlessly integrates conditions and temporal information. This tailored approach ensures the efficient transfer of the diffusion process to the NLVL task. Additionally, we employ multi-scale techniques to enhance performance, facilitating the interaction between query and video data across various temporal scales. Experimental results on the Charades-STA and DiDeMo datasets validate the effectiveness of our innovative design. Our contributions are summarized as follows:

- We propose a novel interpretation of the NLVL task as a diffusion generation problem, specifically focusing on generating multi-scale 2D temporal maps. These maps are conditioned on both video and language inputs. This exploration presents a fresh perspective on applying diffusion models in multimodal understanding tasks.
- We identify a fundamental challenge in directly applying successful diffusion models from generation tasks to NLVL. We demonstrate the infeasibility of transplanting existing diffusion models and highlight the inherent differences between understanding tasks and generative tasks. Then, we design a customized diffusion decoder that incorporates conditions and time information in a novel way specific to NLVL.

2. Related Work

2.1. The NLVL Task

Existing frameworks to solve NLVL can be broadly classified into proposal-based and proposal-free frameworks. Within the proposal-free framework, common approaches include regression and span-based methods. Regression-based methods [5, 18, 36] address video localization by learning cross-modal interactions between video and query, and directly estimate the temporal time of target moment. Span-based methods [9, 13, 38, 39] tackle video localization by adapting the concept of extractive question answering and predicting the start and end boundaries of the target moment directly.

The proposal-based framework encompasses proposal-generated and anchor-based methods. Proposal-generated methods [30–32] solve this task through a two-stage *propose-and-rank* pipeline. That is, proposals are first generated, then multimodal matching is employed to predict the most matching proposal for a given query. Anchor-based methods [29, 35, 42, 43], on the other hand, sequentially assign each frame with multiscale temporal anchors and select the anchor with the highest confidence as the result. Among them, 2D-map methods [29, 42] utilize a two-dimensional map to model temporal relations between pre-generated candidate proposals. The map not only enumerates all possible proposals of any length with respect to a time scale/unit, but also maintains their adjacent relations. Consequently, 2D-map based methods have the advantage of leveraging rich contextual information to refine moment representations.

In this paper, the proposed multi-scale 2D temporal map diffusion model makes an alternative exploration to the NLVL task. It introduces the utilization of a generative diffusion model, which facilitates the progressive refinement of 2D score maps. This innovative approach sets our work apart from existing literature in the field.

2.2. Diffusion Models

The diffusion model [25], originally proposed as a deep latent generative model, has gained significant attention in recent years. Notably, diffusion-based generation has achieved remarkable results for various tasks such as image generation [7, 22], natural language generation [10, 34], and text-to-image synthesis [11, 12]. While diffusion models have demonstrated their effectiveness in generative tasks involving images and audio, their potential in understanding tasks has not been thoroughly explored. Some pioneering studies have made initial attempts to apply diffusion models to tasks such as object detection [6], image segmentation [1, 3], action segmentation [16], and named entity recognition [23]. Most relevant to ours, recent works [14, 44] have attempted to adapt diffusion models to NLVL, using a proposal-free framework and focusing on the start and end locations of target moments as diffusion objectives. Our approach, in

contrast, employs a proposal-based framework to adapt diffusion model, and is trained to predict an entire 2D temporal map. Our diffusion objective thus offers a more informative content representation with continuous values, aligning more closely with the original diffusion formation.

3. Method

This section begins with the formulation of 2D temporal map in Sec. 3.1. Sec. 3.2 then describes the diffusion process applied in generating the 2D temporal map. Subsequently, the framework of the proposed diffusion model is outlined in Sec. 3.3. The detailed training and inference procedures are presented in Sec. 3.4.

3.1. 2D Temporal Map

Let V be an untrimmed video and $S = \{s_i\}_{i=0}^{M-1}$ be a query sentence with M words. The NLVL task is to retrieve a temporal moment (m_s, m_e) on V that semantically corresponds to the query, where m_s and m_e refer to the start and end timestamp of the moment respectively.

Given the definition, one straightforward formulation is to predict the tuple (m_s, m_e), *i.e.,* the start and end timestamps. However, alternative formulations exist. We follow the 2D-map formulation and utilize a 2D temporal score map, denoted by $\boldsymbol{Y}_0$, for moment prediction. To construct this map, we divide the video $V = \{v_i\}_{i=0}^{N-1}$ into N non-overlapping segments each of length τ, using τ as the time unit. Then there is a correspondence between the segment position and timestamp. Specifically, a candidate moment starting from the timestamp $i\tau$ and with a length of $(j+1)\tau$ can be represented by the segment position (i, j) on a 2D map, illustrated in Fig. 1.

The values in the 2D temporal map cells represent the degree of matching between the given sentence and the moment candidates at various (i, j) positions. In our implementation, we utilize the Intersection over Union (IoU) as the matching score. IoU is computed as the ratio of the overlap between a candidate moment and the ground truth moment (m_s, m_e) to their union duration:

$$\boldsymbol{Y}_0^{i,j} = \frac{(i\tau, i\tau + (j+1)\tau) \cap (m_s, m_e)}{(i\tau, i\tau + (j+1)\tau) \cup (m_s, m_e)}. \tag{1}$$

According to [42], aggregating the results of sparse multi-scale score maps yields higher efficiency and superior performance compared to using a dense single-scale map. Thus, we employ a similar approach in our study. Specifically, we generate K multi-scale maps, where the k-th map is extracted from the original single-scale score map at intervals of 2^k in both the row and column dimensions. Under this setting, the model is designed to generate K target 2D score maps simultaneously, which will be consolidated into a single-scale map during inference.

3.2. 2D Temporal Map-based Diffusion Process

Our approach reinterprets the NLVL task as a conditional generation problem, wherein the input video V and textual query S are considered as conditions, and the objective is to generate the target IoU Map $\boldsymbol{Y}_0$. This can be represented as $\hat{\boldsymbol{Y}}_0 = f_\theta(\boldsymbol{Y}_t, t, V, S)$. The form of $\boldsymbol{Y}_0$ can take various variables depending on the specific methodology employed, such as the time step in regression-based methods or the video span in span-based methods. In our case, we opt for utilizing a 2D temporal map as the prediction objective due to its higher informative content, and more importantly, continuous value representation.

We use the Denoising Diffusion Implicit Model (DDIM) [27] for the diffusion process, which consists of two primary components: the *forward* and *reverse* processes.

The forward process is illustrated in Fig. 2 (a), which should be viewed from right to left. Given a data distribution $\boldsymbol{Y}_0 \sim q(\boldsymbol{Y}_0)$, the *forward* process q progressively incorporate Gaussian noise determined by a predefined variance $\beta_t \in (0, 1)$ at each time step t.[1] In this process, it sequentially generates noisy data samples $\boldsymbol{Y}_1, \boldsymbol{Y}_2, ..., \boldsymbol{Y}_T$ as follows:

$$q(\boldsymbol{Y}_{1:T}|\boldsymbol{Y}_0) = \prod_{t=1}^{T} q(\boldsymbol{Y}_t|\boldsymbol{Y}_{t-1}), \tag{2}$$

$$q(\boldsymbol{Y}_t|\boldsymbol{Y}_{t-1}) = \mathcal{N}(\boldsymbol{Y}_t; \sqrt{1-\beta_t}\boldsymbol{Y}_{t-1}, \beta_t \boldsymbol{I}). \tag{3}$$

Meanwhile, it is possible to directly sample data $\boldsymbol{Y}_t$ at any given time step t without the need for recursively applying Eq. (3):

$$q(\boldsymbol{Y}_t|\boldsymbol{Y}_0) = \mathcal{N}\left(\boldsymbol{Y}_t; \sqrt{\bar{\alpha}_t}\boldsymbol{Y}_0, (1-\bar{\alpha}_t)\boldsymbol{I}\right), \tag{4}$$

where $\alpha_t = 1 - \beta_t$ and $\bar{\alpha}_t = \prod_{s=0}^{t} \alpha_s$.

The *reverse* process, illustrated in Fig. 2 (a) progressing from left to right, involves generating $\boldsymbol{Y}_0$ through iterative denoising:

$$\begin{aligned} p_\theta(\boldsymbol{Y}_{t-1}|\boldsymbol{Y}_t) =& \sigma_t \epsilon + \sqrt{\bar{\alpha}_{t-1}} f_\theta(\boldsymbol{Y}_t, t, V, S) + \\ & \sqrt{1-\bar{\alpha}_{t-1}-\sigma_t^2}\frac{\boldsymbol{Y}_t - \sqrt{\bar{\alpha}_t} f_\theta(\boldsymbol{Y}_t, t, V, S)}{\sqrt{1-\bar{\alpha}_t}}. \end{aligned} \tag{5}$$

where σ_t is controlled by β_t, $\epsilon \in \mathcal{N}(0, \boldsymbol{I})$. Our model f_θ is designed to predict $\boldsymbol{Y}_0$ and its prediction is denoted as $\hat{\boldsymbol{Y}}_0 = f_\theta(\boldsymbol{Y}_t, t, V, S)$. For a more detailed illustration of diffusion theory, we refer readers to [27].

3.3. Framework

Our proposed model consists of two main components: a *multimodal feature encoder* and a subsequent *condition-injected decoder*, i.e., $f_\theta = f_\theta^{dec} \circ f_\theta^{enc}$. The encoder functions generate multimodal fused feature, denoted as $\boldsymbol{F}^F$,

[1] The time step t here is specific to the diffusion model, not to be confused with the timestamp or time unit specific to the video input.

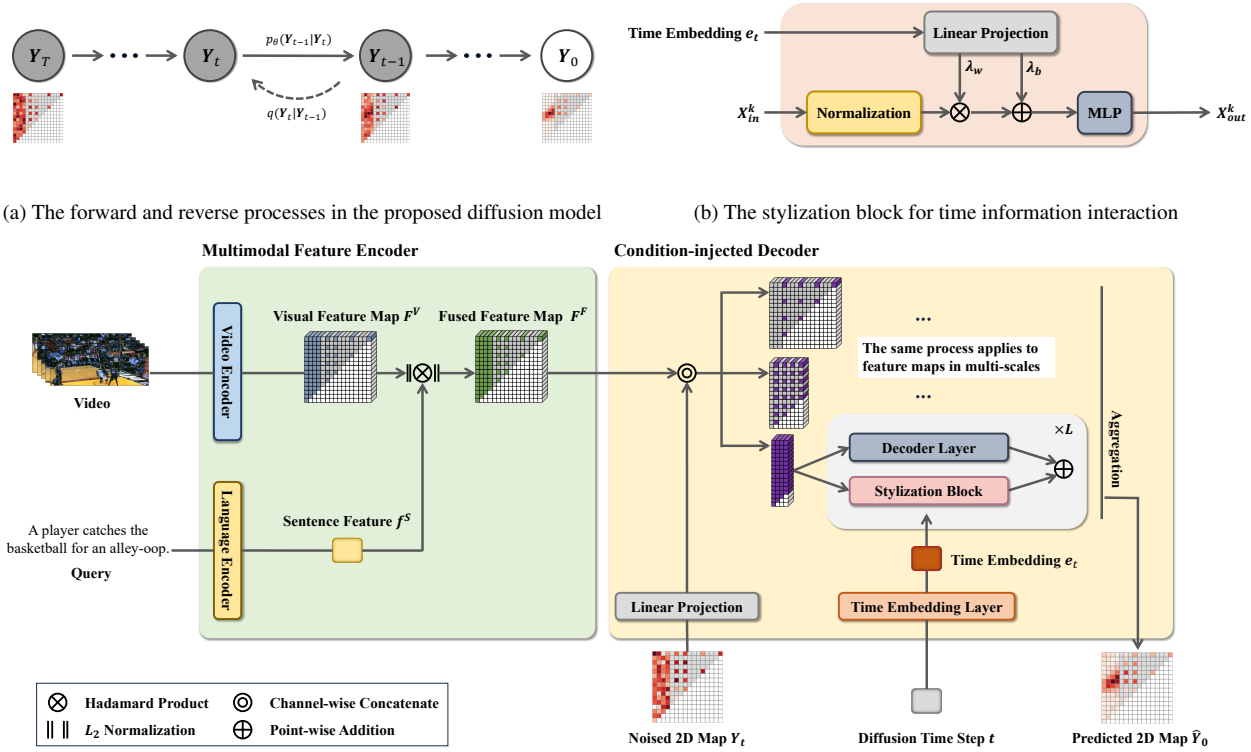

(a) The forward and reverse processes in the proposed diffusion model

(b) The stylization block for time information interaction

(c) The proposed framework: multimodal feature encoder and condition-injected decoder

Figure 2. Overview of our proposed multi-scale 2D temporal map diffusion model. (a) Illustration of the forward and reverse processes in our 2D temporal map-based diffusion model. (b) Design of the stylization block utilized for time information interaction. (c) Framework of the proposed model, incorporating a multimodal feature encoder and a condition-injected decoder.

from both input video segments and query sentences. Then the decoder progressively denoises multi-scale 2D score maps $\boldsymbol{Y}_t$, conditioned on $\boldsymbol{F}^F$. An overview of our framework is presented in Fig. 2 (c).

3.3.1 Multimodal Feature Encoder

The multimodal feature encoder transforms an input video with N segments $V = \{v_i\}_{i=0}^{N-1}$ and a query sentence containing M words $S = \{s_i\}_{i=0}^{M-1}$ into a multimodal fused feature map $\boldsymbol{F}^F$, i.e., $\boldsymbol{F}^F = f_{enc}(V, S)$. We adopt the method in [42] as the main pipeline to generate the fused feature map. Specifically, a visual and text encoder first separately encode the features from the two modalities. Following this, a multimodal feature fusion module is used to generate the fused feature map. The pipeline of the encoder is illustrated in the left part of Fig. 2 (c).

Our implementation utilizes a three-layer bidirectional LSTM network as the text encoder.[2] It receives a sequence of word embedding vectors, generated by the GloVe model [21], and creates an aggregate sentence feature $\boldsymbol{F}^S \in \mathbb{R}^{d_S}$.

The visual encoder initially processes the video segment sequence $\{v_i\}_{i=0}^{N-1}$ into a feature sequence $\{\boldsymbol{f}_i^V\}_{i=0}^{N-1}$ using a pre-trained 3D CNN and a following fully connected layer.[3] Subsequently, a stacked convolution module [37] constructs 2D visual feature maps $\boldsymbol{F}^V \in \mathbb{R}^{N\times N\times d_V}$ from this feature sequence. The dimensions of this map symbolize the start and duration segment indices and the feature dimension. The feature of a moment starting at segment v_a and lasting $(b+1)\tau$ is positioned at $\boldsymbol{F}^V[a, b]$.

The multimodal feature fusion module then integrates the 2D visual feature maps $\boldsymbol{F}^V$ and the sentence feature $\boldsymbol{f}^S$. This fusion module first projects these cross-domain features into a shared subspace using fully connected layers. These are then combined via a Hadamard product and L_2 normalization. The resultant fused feature map, denoted as $\boldsymbol{F}^F \in \mathbb{R}^{N\times N\times d_F}$, carries a feature dimension of d_F.

In our implementation, we construct K multi-scale 2D

[2]The utilization of LSTM aligns with the prevailing approach in NLVL research and contributes to achieving state-of-the-art performance in this task.

[3]Similarly, the utilization of pre-trained 3D CNNs has become a standard practice in NLVL research, showcasing their efficacy and providing a strong foundation for achieving state-of-the-art results in this field.

feature maps to match 2D score maps. The k-th sparse map is sampled from the fused feature map at intervals of 2^k in both the row and column dimensions. We represent the multi-scale feature maps as $\{\boldsymbol{F}_k^F | \boldsymbol{F}_k^F \in \mathbb{R}^{N \times 2^k A \times d_F}, 0 \leq k \leq K-1\}$, where A represents the number of anchors at each scale. Each map is then processed by different decoders with the same architecture.

3.3.2 Condition-injected Decoder

The condition-injected decoder is pivotal in executing the reverse diffusion process. It transforms the noised 2D temporal map, denoted as $\boldsymbol{Y}_t$, into an estimation $\hat{\boldsymbol{Y}}_0$ of the ground truth $\boldsymbol{Y}_0$. This transformation process is conditioned on the multimodal fused feature map $\boldsymbol{F}^F$ and the time step t, mathematically expressed as $\hat{\boldsymbol{Y}}_0 = f_\theta^{dec}(\boldsymbol{Y}_t, t, \boldsymbol{F}^F)$. As depicted in the right part of Fig. 2 (c), the decoder module comprises K decoders, all with identical architecture, operating simultaneously on K multi-scale feature maps. In this section, we detail our design using the pipeline of the k-th decoder as an example. Sec. 3.4 then discuss the aggregation of K predicted 2D score maps into a single-scale map during training and inference respectively.

- **Base Architecture Selection.** As shown in the right part of Fig. 2 (c), the decoder contain L stacked blocks and each blcok contains a main function block and a stylization block. We are here to discuss the architecture selection of the main function block. As depicted in the right part of Fig. 2(c), the decoder comprises L stacked blocks, with each block consisting of a main function block and a stylization block. This part focuses on the architectural choices for the main function block.
  - **Transformer Model.** One straightforward approach to model design is to leverage successful diffusion architectures from existing generation tasks. In this work, we adopt the transformer architecture proposed in [40] as the base diffusion model. To prepare the 2D score map $\boldsymbol{Y}_t^k$ for further processing, it undergoes a transformation through a fully connected layer, resulting in the representation $\boldsymbol{H}_t^k$. This transformed representation is fed into the stacked Transformer blocks for subsequent processing and generation. The Transformer block comprises an attention module and a feed-forward network (FFN). The attention module combines self-attention and cross-attention functionalities. Specifically, it utilizes $\boldsymbol{H}_t^k$ as the query, while the concatenation of $\boldsymbol{H}_t^k$ and $\boldsymbol{F}_k^F$ serves as the key and value. This design allows the layer to simultaneously enhance the interaction between moments and incorporate the conditioning information into the representation of the score map. Following the processing by the Transformer block, the resulting feature will be utilized for predicting $\hat{\boldsymbol{Y}}_0^k$ using a fully connected layer.
  - **Convolution Model.** We also investigate a convolution-based decoder in our design, drawing inspiration from the successful implementation of the 2D convolutional architecture described in [42]. Specifically, we replace the Transformer component with stacked gated convolutional layers [33], utilizing large kernel sizes. This architectural choice allows our model to progressively capture more contextual information from neighboring moment candidates while also learning to differentiate between candidate moments. The convolution model is the default architecture in the main experiments.
- **Approaches of Incorporating Conditions.** One crucial consideration in designing a diffusion model is effectively incorporating the conditioning information with the diffusion target, *i.e.,* the 2D temporal score map in our context.
  - **Cross-attention.** Adopting successful interaction methods from other generation tasks, we utilize cross-attention in a Transformer architecture, as proposed in Zhang et al. [40]. This architecture integrates both self-attention and cross-attention functionalities within its attention layer. In this design, the noised 2D temporal map $\boldsymbol{Y}_t^k \in \mathbb{R}^{N \times 2^k A}$ is initially projected to $\boldsymbol{H}_t^k \in \mathbb{R}^{N \times 2^k A \times d_{\boldsymbol{H}_t^k}}$ using a fully connected layer. Then, $\boldsymbol{H}_t^k$ serves as the query, and the concatenation of $\boldsymbol{H}_t^k$ and $\boldsymbol{F}_k^F$ acts as the key and value. This configuration allows the layer to not only enhance interactions between different moments but also integrate conditioning information into the score map representation.
  - **Direct Concatenation.** However, the inherent differences between generation and understanding tasks are significant. Generation tasks focus on adhering to given conditions while ensuring diversity in outputs, often without a definitive ground truth for evaluation, thus rely less on conditional information. In contrast, our NLVL task demands the precise generation of predetermined results, necessitating effective leverage of input conditions from both modalities. This requirement suggests that typical interaction mechanisms like plain cross-attention may not be optimal, as supported by findings in Sec. 4.3.1. Consequently, we propose a more direct approach for our NLVL task. This involves processing the concatenation of the condition and projected diffusion target ($[\boldsymbol{H}_t^k, \boldsymbol{F}_k^F]$) together during the denoising process. In the Transformer model, the original attention layer is replaced with a general self-attention layer, using $[\boldsymbol{H}_t^k, \boldsymbol{F}_k^F]$ as the query, key, and value. For the CNN model, this concatenated input is used in the forward pass.
- **Time Information Interaction.**
  - **Stylization Block.** Incorporating time step information is essential throughout the denoising process. To facilitate this, we introduce *stylization blocks* within the residual branch, designed to apply a stylization effect on

the inputs, as depicted in Fig. 2(b). The diffusion time step t is initially processed by a time embedding layer, yielding the time embedding e_t. The stylization block employs a linear projection to transform e_t into two vectors, λ_w and λ_b, representing the scale and shift values for the stylization process, respectively. The input to the stylization block, denoted as X^k_{in}, is generated from the preceding layer, while X^k_{out} represents its output. Initially, X^k_{in} is normalized using GroupNorm in CNN models, or LayerNorm in Transformer models. Subsequently, it undergoes stylization through λ_w and λ_b. Finally, a multilayer perceptron (MLP) with a preceding activation function is utilized to generate the output of the stylization block. Thus, the overall process can be mathematically formulated as follows:

$$X^k_{out} = \text{MLP}\left(\text{Norm}(X^k_{in}) \cdot \lambda_w + \lambda_b\right), \quad (6)$$

where $[\lambda_w, \lambda_b] = \text{Proj}(e_t)$.

– **Multi-step Interaction.** To ensure that the time step information has a meaningful influence on the generated outputs, we incorporate a stylization block after every layer. Specifically, in the Transformer block, we place the stylization block after the attention module and the feed-forward network (FFN). As for the CNN model, we position the stylization block at the beginning and after each convolutional layer, respectively. This placement ensures that the time step information is effectively integrated at different stages of the denoising process.

3.4. Training and Inference

In this section, we elucidate how predictions from different decoders are utilized during the training and inference stages.

Our model f_θ is designed to predict $\boldsymbol{Y}_0$. Therefore, in the *training* stage, it is trained to align its prediction $\hat{\boldsymbol{Y}}_0 = f_\theta(\boldsymbol{Y}_t, t, V, S)$ with the groud truth $\boldsymbol{Y}_0$. Since K multi-scale 2D feature maps are used for prediction, we generate corresponding multi-scale noised 2D temporal maps $\{\boldsymbol{Y}^k_t\}^{K-1}_{k=0}$ via Eq. (4) and the time step t is randomly selected at each training iteration. As for the loss selection, we choose to utilize the original 2D temporal map as the ground truth and employ mean squared error (MSE) for optimization. The training loss is defined as:

$$\mathcal{L} = \Sigma^{K-1}_{k=0} \mathcal{L}^k, \quad (7)$$

$$\mathcal{L}^k = \mathbb{E}_{t\sim[1,T],\boldsymbol{Y}_0\sim q(\boldsymbol{Y}_0),\epsilon\in\mathcal{N}(0,\boldsymbol{I})}[\|f_\theta(\boldsymbol{Y}^k_t, t, V, S) - \boldsymbol{Y}^k_0\|_2], \quad (8)$$

where K is the total number of 2D maps. Note that, in MS-2D-TAN [42], a rescaled 2D map and binary cross-entropy (BCE) are used as the prediction objective and training loss, respectively. However, rescaling the 2D map can result in increased sparsity and reduced informativeness. Additionally, the utilization of BCE assumes a discrete prediction objective, which contradicts the continuity requirement in the original DDIM. Hence, we choose differently.

During the *inference stage*, the model begins with pure noise maps, $\{\boldsymbol{Y}^k_T \sim \mathcal{N}(0, \boldsymbol{I})\}^{K-1}_{k=0}$, and progressively reduces the noise via Eq. (5). Then, all denoised score maps $\{\hat{\boldsymbol{Y}}^k_0\}^{K-1}_{k=0}$ are recovered to a single-scale map $\hat{\boldsymbol{Y}}_0$ based on the moment location at the original single-scale map. For moments that are predicted by more than one score map, we choose the highest score as its final prediction.

4. Experiment

4.1. Experimental Setting

- **Datasets.** Our experiments employ the Charades-STA [8] and DiDeMo [2] datasets. The Charades-STA dataset, derived from the original Charades dataset [24], features $9,848$ videos that depict common indoor activities. This dataset includes $16,128$ moment-language query pairs, with $12,408$ pairs designated for training and $3,720$ for testing. The average lengths of videos and moments are 30.60 seconds and 8.09 seconds, respectively. The DiDeMo dataset provides a comprehensive and diverse assortment of videos from Flickr, with a specific focus on event localization through natural language descriptions. The videos, each restricted to maximum 30 seconds, are divided into 5-second segments to facilitate easier annotation. The dataset encompasses $8,395$ training videos, $1,065$ validation, and $1,004$ test videos, resulting in a total of $26,892$ moment-description pairs.
- **Evaluation Metrics.** We follow the evaluation framework of [42] for assessing the performance of our model, employing the $Rank\ n@m$ metric. This metric is derived by determining the percentage of language queries where at least one *accurate moment retrieval* appears within the top-n retrieved moments. A moment retrieval is considered *accurate* if its Intersection over Union (IoU) with the ground truth moment exceeds the threshold m. The specific combinations for n and m may differ between datasets. For both Charades-STA and DiDeMo datasets, we report results with $n \in \{1, 5\}$ and $m \in \{0.5, 0.7\}$.

4.2. Performance Comparison

We compare our CNN-based diffusion model and other state-of-the-art models. The evaluation results on the Charades-STA dataset are outlined in Tab. 1. Notably, our model demonstrates exceptional performance, surpassing other models in both top-1 and top-5 prediction measures when $m = 0.7$. This enhancement is particularly remarkable contrasting the outcomes with MS-2D-TAN.

The core of our model is an iterative diffusion process which starts from a pure noise state and progressively denoises it, resulting in a 2D temporal map of higher accuracy than those generated by the single inference processes typi-

Method	Feature	Rank1@		Rank5@	
		0.5	0.7	0.5	0.7
LGI [19]	I3D	59.5	35.5	-	-
VSLNet [38]	I3D	54.2	35.2	-	-
IVG-DCL [20]	I3D	50.2	32.9	-	-
ACRM [28]	I3D	57.5	38.3	-	-
GTR-H [4]	RAW	62.6	39.7	91.6	62.0
CTRL [8]	C3D	23.6	8.9	58.9	29.6
QSPN [32]	C3D	35.6	15.8	79.4	45.5
2D-TAN [41]	VGG	39.8	23.3	79.3	51.2
BPNet [31]	I3D	50.8	31.6	-	-
SCDM [35]	I3D	54.4	33.4	74.4	58.1
MS-2D-TAN [42]	I3D	60.1	37.4	89.1	59.2
Ours	I3D	60.3	40.8	79.7	63.0

Table 1. Performance on Charades-STA. Results of other models are obtained from their original papers.

Method	Feature	Rank1@		Rank5@	
		0.5	0.7	0.5	0.7
ACRN [17]	VGG	27.4	16.7	69.4	29.5
CSMGAN [15]	C3D	29:4	19.2	70.8	41.6
VLG-Net [26]	VGG	33.4	25.6	88.7	71.7
MS-2D-TAN [42]	VGG	26.1	23.0	76.1	63.6
Ours	VGG	31.5	25.3	72.1	65.4

Table 2. Performance on DiDeMo. Results of other models are obtained from their original papers, except MS-2D-TAN, which are obtained in our experiments.

cal in discriminative models. This improvement underscores the potency of diffusion models in tasks requiring deep understanding, especially when they are adeptly designed to exploit multi-modal conditions. The success of our model in these respects indicates that our diffusion model architecture is not only well-suited but also excels in the task of NLVL.

In Tab. 2, we observe that the original MS-2D-TAN model performs poorly as a strong baseline model on the DiDeMo dataset. However, using the same convolution architecture, our diffusion model outperforms it on 3 out of 4 measures. This suggests that the diffusion model has the potential to consistently enhance performance across different datasets.

4.3. Ablation Study

4.3.1 Approaches of Incorporating Conditions

As part of our initial investigation, we evaluated various strategies for introducing conditional information into the denoising process. For Transformer-based models, we experimented with integrating the conditioning information into the diffusion target via both *cross-attention* mechanisms and *concatenation*. With cross-attention, we not only processed multi-scale 2D maps separately but also combined them into a single sequence, referred to as *single-scale*. In the context of CNN models, we examined several alternatives, including different *multiplicative* interactions between the score map and the feature map for enhanced denoising. Among many experiments conducted, we only list the best results obtained on the Charades-STA dataset here. Tab. 3 reveals that the concatenation method outperforms others with both Transformer and CNN frameworks. This underscores the indispensable role of conditional information in

Architecure	Approach	Rank1@		Rank5@	
		0.5	0.7	0.5	0.7
Transformer	x-attn + ss	37.0	20.2	59.4	38.4
Transformer	x-attn	40.8	22.3	64.0	43.0
Transformer	concat	53.2	32.1	72.0	50.3
CNN	mul	57.9	37.0	79.1	57.7
CNN	concat	60.3	40.8	79.7	63.0

x-attn: cross-attention; **ss**: single-scale; **concat**: concatenation; **mul**: multiplication.

Table 3. Ablation study on condition incorporation methods on the Charades-STA dataset. Results indicate that the concatenation approach in condition interaction yields best performance.

Loss Type	2D Map Type	Rank1@		Rank5@	
		0.5	0.7	0.5	0.7
BCE	rescaled map	56.6	39.5	84.2	61.3
BCE	full map	58.6	38.3	79.1	58.6
MSE	full map	60.3	40.8	79.7	63.0

Table 4. Ablation study on optimization objective design on the Charades-STA dataset. Results show that integrating mean squared error (MSE) loss with full 2D score map improves the generation objective and optimizes the diffusion process.

Fusion Layer	Conv Layer	Rank1@		Rank5@	
		0.5	0.7	0.5	0.7
- stylization	- stylization	59.1	37.4	81.5	57.7
+ stylization	- stylization	60.2	39.0	80.4	59.3
- stylization	+ stylization	59.7	38.4	79.9	58.6
+ stylization	+ stylization	60.3	40.8	79.7	63.0

Table 5. Ablation Study on Time Information Interaction. Symbols + and - indicate with and without stylization blocks in the corresponding layer. Findings indicate that stylization blocks at any position improve performance, with the best results achieved when all blocks are active, underscoring the value of multi-step temporal interaction for denoising 2D temporal maps.

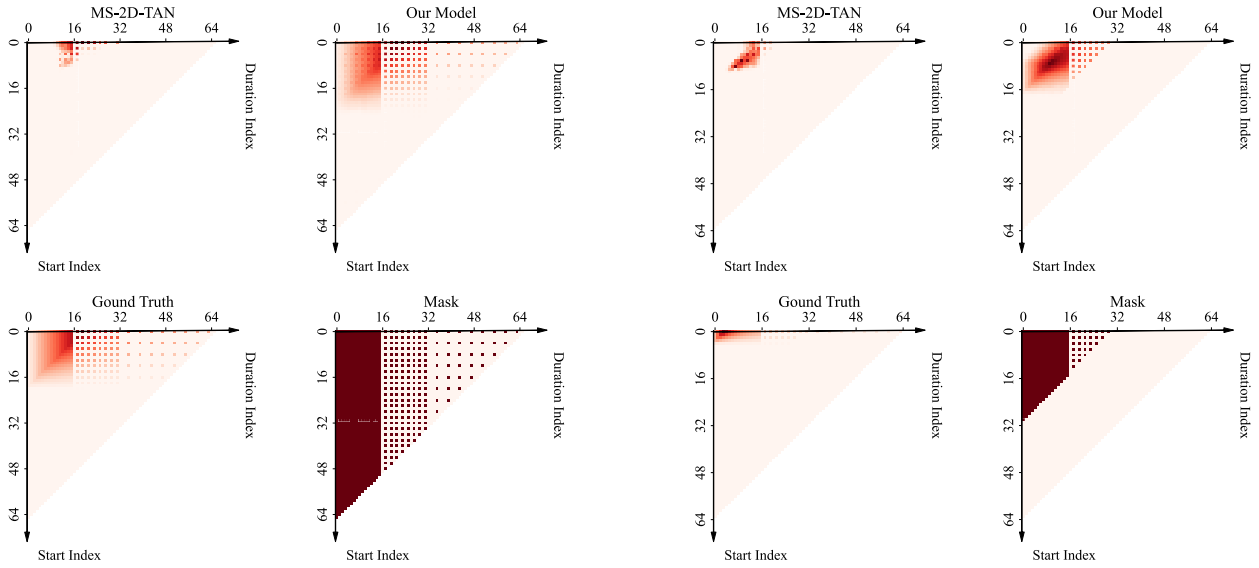

(a) Sample of correct prediction

(b) Sample of wrong prediction

Figure 3. Visualizations of predicted 2D maps for two samples (from Charades-STA), generated by the MS-2D-TAN model and our diffusion model. The diffusion model consistently produces 2D maps with a recognizable pattern, despite occasional incorrect predictions.

understanding-oriented tasks for making precise predictions. Consequently, our findings confirm the effectiveness of the concatenation approach in condition interaction for optimal performance in NLVL tasks.

In addition, also observe in Tab. 3 that the CNN-based diffusion model outperforms its Transformer-based counterpart. This superior performance is primarily attributed to the inductive bias of the convolutional model. It facilitates the progressive capture of contextual information, starting from neighboring moments and extending across all candidates. In contrast, the Transformer model processes all moments simultaneously from the input layer, which hinders the model's ability to effectively differentiate between adjacent moments.

4.3.2 Design of Optimization Objective

To validate the soundness of our chosen optimization objective, we executed a series of experiments examining various combinations of loss functions and 2D map configurations. The findings, reported in Tab. 4, indicate that our proposed approach surpasses competing methods on most measures. This substantiates our initial premise that the application of mean squared error (MSE) loss in conjunction with a full 2D score map constitutes a more informative generative objective. Such an objective is demonstrably more conducive to the diffusion process, aligning with the generative nature of the task at hand.

4.3.3 Time Information Interaction

We additionally evaluated the impact of diffusion time step interactions on our model's performance. In the control experiments, we systematically removed stylization blocks from various positions within the architecture, as indicated in Tab. 5. A comparative analysis between the baseline (first row) and subsequent configurations (following rows) reveals that the inclusion of stylization blocks in both layers contributes to improved performance. Notably, the model exhibits peak performance when all stylization blocks are operational, signifying the advantage of multi-step temporal information interaction. These findings corroborate the efficacy of stylization blocks in infusing time step information into the denoising process of 2D temporal maps.

4.4. Qualitative Result

In Fig. 3, we present visualizations of the predicted 2D maps generated by both the MS-2D-TAN model and our diffusion model alongside the ground truth. Upon comparing these visualizations, it becomes evident that the diffusion model produces 2D maps with a consistent pattern, although the predictions may not be entirely correct. Specifically, the diffusion model tends to generate a plausible distribution (values decrease when they get far from the predicted center), even when the center of the heat map is incorrectly located. In contrast, the quality of the 2D maps generated by the MS-2D-TAN model is subpar, even when the top-1 prediction is accurate.

5. Conclusion

In this study, we redefine the NLVL task as a conditional diffusion generation challenge, focusing on creating a global 2D temporal map to better capture temporal dynamics. We identify key differences between generative and understanding tasks, and particularly in the context of NLVL. We then develop a specialized diffusion decoder tailored for NLVL, incorporating conditions and diffusion time steps. The main modifications include altering the base architecture, refining the integration of conditions, enhancing the interaction with time information, and designing optimization objective. These changes resulted in improved feature modeling and a more suitable diffusion process for the NLVL task. Experiments confirmed the effectiveness of our design, highlighting the unique characteristics of our diffusion model. We believe this work offers a fresh perspective on utilizing diffusion models in multimodal understanding tasks and could serve as a guide for future innovations in this field.

References

[1] Tomer Amit, Tal Shaharbany, Eliya Nachmani, and Lior Wolf. Segdiff: Image segmentation with diffusion probabilistic models. *arXiv preprint arXiv:2112.00390*, 2021. 2

[2] Lisa Anne Hendricks, Oliver Wang, Eli Shechtman, Josef Sivic, Trevor Darrell, and Bryan Russell. Localizing moments in video with natural language. In *ICCV*, pages 5803–5812, 2017. 6

[3] Dmitry Baranchuk, Ivan Rubachev, Andrey Voynov, Valentin Khrulkov, and Artem Babenko. Label-efficient semantic segmentation with diffusion models. *arXiv preprint arXiv:2112.03126*, 2021. 2

[4] Meng Cao, Long Chen, Mike Zheng Shou, Can Zhang, and Yuexian Zou. On pursuit of designing multi-modal transformer for video grounding. In *EMNLP*, pages 9810–9823. Association for Computational Linguistics, 2021. 7

[5] Long Chen, Chujie Lu, Siliang Tang, Jun Xiao, Dong Zhang, Chilie Tan, and Xiaolin Li. Rethinking the bottom-up framework for query-based video localization. In *AAAI*, pages 10551–10558. AAAI Press, 2020. 1, 2

[6] Shoufa Chen, Peize Sun, Yibing Song, and Ping Luo. Diffusiondet: Diffusion model for object detection. *arXiv preprint arXiv:2211.09788*, 2022. 2

[7] Prafulla Dhariwal and Alexander Nichol. Diffusion models beat gans on image synthesis. *NeurIPS*, 34:8780–8794, 2021. 2

[8] Jiyang Gao, Chen Sun, Zhenheng Yang, and Ram Nevatia. TALL: temporal activity localization via language query. In *ICCV*, pages 5277–5285. IEEE Computer Society, 2017. 6, 7

[9] Soham Ghosh, Anuva Agarwal, Zarana Parekh, and Alexander Hauptmann. Excl: Extractive clip localization using natural language descriptions. *arXiv preprint arXiv:1904.02755*, 2019. 1, 2

[10] Shansan Gong, Mukai Li, Jiangtao Feng, Zhiyong Wu, and LingPeng Kong. Diffuseq: Sequence to sequence text generation with diffusion models. *arXiv preprint arXiv:2210.08933*, 2022. 2

[11] Shuyang Gu, Dong Chen, Jianmin Bao, Fang Wen, Bo Zhang, Dongdong Chen, Lu Yuan, and Baining Guo. Vector quantized diffusion model for text-to-image synthesis. In *CVPR*, pages 10696–10706, 2022. 2

[12] Gwanghyun Kim, Taesung Kwon, and Jong Chul Ye. Diffusionclip: Text-guided diffusion models for robust image manipulation. In *CVPR*, pages 2426–2435, 2022. 2

[13] Jie Lei, Licheng Yu, Tamara L Berg, and Mohit Bansal. Tvr: A large-scale dataset for video-subtitle moment retrieval. In *ECCV*, pages 447–463. Springer, 2020. 1, 2

[14] Pandeng Li, Chen-Wei Xie, Hongtao Xie, Liming Zhao, Lei Zhang, Yun Zheng, Deli Zhao, and Yongdong Zhang. Momentdiff: Generative video moment retrieval from random to real. In *NeurIPS*, 2023. 2

[15] Daizong Liu, Xiaoye Qu, Xiao-Yang Liu, Jianfeng Dong, Pan Zhou, and Zichuan Xu. Jointly cross-and self-modal graph attention network for query-based moment localization. In *ACM MM*, pages 4070–4078, 2020. 7

[16] Daochang Liu, Qiyue Li, AnhDung Dinh, Tingting Jiang, Mubarak Shah, and Chang Xu. Diffusion action segmentation. *arXiv preprint arXiv:2303.17959*, 2023. 2

[17] Meng Liu, Xiang Wang, Liqiang Nie, Xiangnan He, Baoquan Chen, and Tat-Seng Chua. Attentive moment retrieval in videos. In *SIGIR*, pages 15–24, 2018. 7

[18] Chujie Lu, Long Chen, Chilie Tan, Xiaolin Li, and Jun Xiao. Debug: A dense bottom-up grounding approach for natural language video localization. In *EMNLP*, pages 5144–5153, 2019. 1, 2

[19] Jonghwan Mun, Minsu Cho, and Bohyung Han. Local-global video-text interactions for temporal grounding. In *CVPR*, pages 10810–10819, 2020. 7

[20] Guoshun Nan, Rui Qiao, Yao Xiao, Jun Liu, Sicong Leng, Hao Zhang, and Wei Lu. Interventional video grounding with dual contrastive learning. In *CVPR*, pages 2765–2775, 2021. 7

[21] Jeffrey Pennington, Richard Socher, and Christopher D Manning. Glove: Global vectors for word representation. In *EMNLP*, pages 1532–1543, 2014. 4

[22] Robin Rombach, Andreas Blattmann, Dominik Lorenz, Patrick Esser, and Björn Ommer. High-resolution image synthesis with latent diffusion models. In *CVPR*, pages 10684–10695, 2022. 2

[23] Yongliang Shen, Kaitao Song, Xu Tan, Dongsheng Li, Weiming Lu, and Yueting Zhuang. Diffusionner: Boundary diffusion for named entity recognition. *arXiv preprint arXiv:2305.13298*, 2023. 2

[24] Gunnar A. Sigurdsson, Gül Varol, Xiaolong Wang, Ali Farhadi, Ivan Laptev, and Abhinav Gupta. Hollywood in homes: Crowdsourcing data collection for activity understanding. In *ECCV*, pages 510–526. Springer, 2016. 6

[25] Jascha Sohl-Dickstein, Eric Weiss, Niru Maheswaranathan, and Surya Ganguli. Deep unsupervised learning using nonequilibrium thermodynamics. In *ICML*, pages 2256–2265. PMLR, 2015. 2

[26] Mattia Soldan, Mengmeng Xu, Sisi Qu, Jesper Tegner, and Bernard Ghanem. Vlg-net: Video-language graph matching network for video grounding. In *ICCV*, pages 3224–3234, 2021. 7

[27] Jiaming Song, Chenlin Meng, and Stefano Ermon. Denoising diffusion implicit models. In *ICLR*, 2021. 3

[28] Haoyu Tang, Jihua Zhu, Meng Liu, Zan Gao, and Zhiyong Cheng. Frame-wise cross-modal matching for video moment retrieval. *IEEE TMM*, 24:1338–1349, 2021. 7

[29] Hao Wang, Zheng-Jun Zha, Liang Li, Dong Liu, and Jiebo Luo. Structured multi-level interaction network for video moment localization via language query. In *CVPR*, pages 7026–7035, 2021. 2

[30] Shaoning Xiao, Long Chen, Jian Shao, Yueting Zhuang, and Jun Xiao. Natural language video localization with learnable moment proposals. *arXiv preprint arXiv:2109.10678*, 2021. 1, 2

[31] Shaoning Xiao, Long Chen, Songyang Zhang, Wei Ji, Jian Shao, Lu Ye, and Jun Xiao. Boundary proposal network for two-stage natural language video localization. In *AAAI*, pages 2986–2994, 2021. 7

[32] Huijuan Xu, Kun He, Bryan A. Plummer, Leonid Sigal, Stan Sclaroff, and Kate Saenko. Multilevel language and vision integration for text-to-clip retrieval. In *AAAI*, pages 9062–9069. AAAI Press, 2019. 1, 2, 7

[33] Jiahui Yu, Zhe Lin, Jimei Yang, Xiaohui Shen, Xin Lu, and Thomas S Huang. Free-form image inpainting with gated convolution. In *CVPR*, pages 4471–4480, 2019. 5

[34] Peiyu Yu, Sirui Xie, Xiaojian Ma, Baoxiong Jia, Bo Pang, Ruigi Gao, Yixin Zhu, Song-Chun Zhu, and Ying Nian Wu. Latent diffusion energy-based model for interpretable text modeling. *arXiv preprint arXiv:2206.05895*, 2022. 2

[35] Yitian Yuan, Lin Ma, Jingwen Wang, Wei Liu, and Wenwu Zhu. Semantic conditioned dynamic modulation for temporal sentence grounding in videos. In *NeurIPS*. Curran Associates, Inc., 2019. 2, 7

[36] Yitian Yuan, Tao Mei, and Wenwu Zhu. To find where you talk: Temporal sentence localization in video with attention based location regression. In *AAAI*, pages 9159–9166, 2019. 1, 2

[37] Da Zhang, Xiyang Dai, Xin Wang, Yuan-Fang Wang, and Larry S Davis. Man: Moment alignment network for natural language moment retrieval via iterative graph adjustment. In *CVPR*, pages 1247–1257, 2019. 4

[38] Hao Zhang, Aixin Sun, Wei Jing, and Joey Tianyi Zhou. Span-based localizing network for natural language video localization. In *ACL*, pages 6543–6554. Association for Computational Linguistics, 2020. 1, 2, 7

[39] Hao Zhang, Aixin Sun, Wei Jing, Liangli Zhen, Joey Tianyi Zhou, and Rick Siow Mong Goh. Natural language video localization: A revisit in span-based question answering framework. *IEEE TPAMI*, 44(8):4252–4266, 2021. 1, 2

[40] Mingyuan Zhang, Zhongang Cai, Liang Pan, Fangzhou Hong, Xinying Guo, Lei Yang, and Ziwei Liu. Motiondiffuse: Text-driven human motion generation with diffusion model. *arXiv preprint arXiv:2208.15001*, 2022. 5

[41] Songyang Zhang, Houwen Peng, Jianlong Fu, and Jiebo Luo. Learning 2d temporal adjacent networks for moment localization with natural language. In *AAAI*, pages 12870–12877, 2020. 7

[42] Songyang Zhang, Houwen Peng, Jianlong Fu, Yijuan Lu, and Jiebo Luo. Multi-scale 2d temporal adjacency networks for moment localization with natural language. *IEEE TPAMI*, 44 (12):9073–9087, 2022. 2, 3, 4, 5, 6, 7

[43] Zhu Zhang, Zhijie Lin, Zhou Zhao, and Zhenxin Xiao. Cross-modal interaction networks for query-based moment retrieval in videos. In *SIGIR*, pages 655–664. ACM, 2019. 2

[44] Henghao Zhao, Kevin Qinghong Lin, Rui Yan, and Zechao Li. Diffusionvmr: Diffusion model for video moment retrieval, 2023. 2